Electronic Supplementary Material (ESI) for Lab on a Chip.

Supplementary Information

MagPure chip: an immunomagnetic-based microfluidic device for high purification of circulating tumor cells from liquid biopsies

Lucie Descamps[a], Jessica Garcia[b], David Barthelemy[b], Emmanuelle Laurenceau[c], Léa Payen[b], Damien Le Roy*[d] and Anne-Laure Deman*[a]

[a] Univ Lyon, Université Claude Bernard Lyon 1, CNRS, INSA Lyon, Ecole Centrale de Lyon, CPE Lyon, INL, UMR5270, 69622 Villeurbanne, France.

[b] Laboratoire de Biochimie et Biologie Moléculaire, CICLY UR3738, Groupe Hospitalier Sud, Hospices Civils de Lyon, 69495 Pierre Bénite, France.

[c] Univ Lyon, Ecole Centrale de Lyon, CNRS, INSA Lyon, Université Claude Bernard Lyon 1, CPE Lyon, CNRS, INL, UMR5270, 69130 Ecully, France.

[d] Univ Lyon, Université Claude Bernard Lyon 1, CNRS, UMR5306 Institut Lumière Matière, 69100 Villeurbanne, France.

*Corresponding authors: damien.le-roy@univ-lyon1.fr; anne-laure.deman-him@univ-lyon1.fr

SI Experimental section

S1. ClearCell FX1 system information

ClearCell® FX1 instrument (Biolidics Ltd, Singapore, BIOSCIENCES®) relies on the Dean Flow Fractionation (DFF) separation technology in a spiral chip. The CTC size cutoff was set to 14 µm but this value can be adjusted by altering the flow ratios at the output to enrich CTCs at a lower cell size [23]. Depending on the desired application, two separation modes depending on CTC size cutoff were therefore developed by Biolidics: P1 (14 µm size cutoff) and P3 (size cutoff <14 µm) running programs. P1 yields recovery rates comprised between 40 and 60% [7], [8] depending on cell type (and therefore on cell size), with a total WBC background of 16,666 WBCs (internal data, median obtained in 8 patient samples with head and neck cancer or NSCLC). P3 allows for higher recovery rates, comprised between 60 and 80% [8], [9], but results in a larger background of WBCs with 300,000 remaining WBCs (internal data, median obtained in 21 patient samples with head and neck cancer or NSCLC. The enrichment step using P1 is performed in 60 minutes while the processing time using P3 is 30 minutes.

S2. Optimization of the magnetic labeling of WBCs

WBCs were collected from a whole blood sample after red blood cell lysis and then labeled with the functionalized magnetic nanoparticles at an optimized concentration of 400 NP/WBC and 100 NP/WBC for anti-CD45- and anti-CD15-conjugated nanoparticles, respectively. WBCs and functionalized nanoparticles were added in PBS supplemented with 2 mM ethylene diamine tetra-acetic acid (EDTA) and 2% bovine serum albumin (BSA) at a volume of 300 µL (injected volume within the chip) and incubated in a 24-well plate (CytoOne®) at 37°C for 30 min under a gentle vortex agitation of 200 rpm (MS-100 Thermoshaker Incubator, Labgene). For experiments requiring fluorescent discrimination, WBCs were stained with Hoechst (Ready Flow Reagent™, Invitrogen) by adding one drop of the dye to the solution of WBCs and NPs within the well, before the incubation.
The final labeling conditions cited above have required a prior optimization. Indeed, several parameters come into play during the labeling process: temperature, agitation, duration, nanoparticle (NP) concentration, as well as suspension medium. Studied parameters are reported in Table 1. In the literature, various magnetic labeling conditions are reported, mostly partially, therefore careful optimization of these variables was necessary for the specific application described here. The optimized conditions were assessed from fluorescence measurements of the WBC (stained nucleus) functionalized with magnetic nanoparticles (conjugated to AlexaFluor-647 fluorophore).

Table S1. Studied parameters for WBC magnetic labeling.

Parameter	Temperature	Agitation	Duration	Nanoparticle concentration	Medium	Antibodies
Tested conditions	- TA - 37˚C	- Without - With	- 2h - 30min	- 100 NP/WBC - 200 NP/WBC - 500 NP/WBC	- PBS - EDTA	- Anti-CD45 - Anti-CD15

First, the temperature was set so as to maintain a good cell viability. WBC viability was 30% higher for the incubation at 37°C. The incubation temperature was then fixed at 37°C.

Regarding the nanoparticle concentration, the theoretical limit for a monolayer coating of particles around WBCs was calculated. Since WBCs have a diameter size range of 8–12µm, their surface area, $4\pi r^2$, is comprised between 201-452 µm². Thus, the maximum number of 0.5-µm diameter particles that can be packed around a single WBC in a closest-packed lattice

with an area per bead of $\sqrt{3}d^2/2$ [1] will range from 900 to 2000. Nevertheless, in the literature has been reported an actual ratio of 5-50 particles per WBC for bigger particles of 1 µm in diameter [2], [3]. Thus, initial nanoparticle concentrations of 100 NP/WBC and 200 NP/WBC were tested. WBCs with nanoparticles were incubated at 37°C for 2h. Results are summarized in Table 2, for nanoparticles conjugated to anti-CD45, anti-CD15 or both anti-CD45 and anti-CD15. The condition 200 NP/WBC with both anti-CD45 and anti-CD15 antibodies (400 NP/WBC in total) returns the highest labeling rate, of 87%.

Table S2. Labeling rate for different NP-to-WBC ratio conditions at different incubation conditions, either 37°C, 2h, without agitation; or 37°C, 30min, with agitation.

Incubation	NP-TO-WBC RATIO		LABELING RATE (%)
	Anti-CD45	Anti-CD15	
37°C - 2h - no agitation	100 NP/WBC	–	70
	100 NP/WBC	100 NP/WBC	78
	200 NP/WBC	–	77
	200 NP/WBC	200 NP/WBC	87
37°C - 30min - 200 rpm agitation	100 NP/WBC	100 NP/WBC	50
	500 NP/WBC	500 NP/WBC	82
	250 NP/WBC	250 NP/WBC	81
	400 NP/WBC	100 NP/WBC	85

Nevertheless, an incubation time of 2 hours could be too long for CTCs and may degrade them, especially since this preparation time is part of a two-step workflow and recovered CTCs must be kept alive for further characterization. Thus, a lower duration was investigated, and agitation was added to enhance WBC and NP interactions. WBCs and nanoparticles were incubated for 30 min on a microplate thermoshaker with heating at 37°C and agitation at 200 rpm. It resulted in a labeling rate of 81% for the concentration of 250 NP/WBC for both antibodies. Despite the slightly lower rate in comparison with the previous 87% labeling rate obtained with a 2h incubation time and a smaller number of NP/WBC, the priority is to preserve CTC viability. Reducing the labeling duration to 30 min was therefore a good compromise. Finally, in order to take into account the heterogeneity of CD45 expression among WBCs in circulation, CD15 marker was also targeted. For optimization experiments, anti-CD45 and anti-CD15 were set in the same proportions but CD45 is actually majorly expressed. Thus, a final NP-to-WBC ratio was fixed at 400 NP/WBC for anti-CD45 antibody and 100 NP/WBC for anti-CD15 antibody. A labeling rate as high as 85% could be reached with this ratio. Interestingly, using only anti-CD45-conjugated nanoparticles in a ratio of 400 NP/WBC resulted in a labeling rate of 63%, which confirms the importance of combining both anti-CD45 and anti-CD15 antibodies to target a maximum of WBC population.

Besides, it is worth mentioning that the medium had also to be optimized. Indeed, WBCs were initially labeled in a PBS solution, but it appeared that after a certain time of incubation WBCs would aggregate to each other, resulting in channel clogging during injection. To prevent WBCs from aggregating, the PBS solution was supplemented with 2 mM EDTA and 2% BSA. EDTA is often encountered in cell preparation protocol to prevent cation-dependent cell-cell adhesion [4]–[6]. A summary of the labeling rate achieved for all of the mentioned conditions is reported in Table 2.

S3. Two-step separation process for whole blood sample processing

Blood samples were obtained from healthy blood donors and collected in 10 mL K2 EDTA tubes (Tubes BD Vacutainer®). First, 20 000 A549 were spiked into 7.5 mL of whole blood and loaded into a new input tube (Corning® 50 mL centrifuge tube). Next, 22.5 mL of lysis buffer was added to the blood sample and RBC lysis was performed. After the centrifugation step and the removal of lysed RBCs, the cell pellet (composed of WBCs and A549 cells) was resuspended is 4 mL of resuspension buffer provided by Biolidics Ltd (ref CBB-F016003). Before proceeding to the size-based enrichment step, any bubbles present within the sample should be carefully removed without discarding the sample volume. Then, the sample was processed on the ClearCell® FX-1 system (using enrichment programs P1 or P3) and collected in an output tube (Falcon® 15 mL centrifuge tube). After the enrichment program, the mCTC-enriched sample was centrifuged at 500g for 10 min, and then resuspended in 300 µL of 2 mM EDTA diluted in PBS-2% BSA. Afterwards, cell viability was accessed by Trypan blue (Gibco, 15250-061) in a 1:1 volume ratio and counting performed in KOVA® slide. The number of total cells and alive cells was reported as a characteristic data of the ClearCell FX1 system separation. In particular, the number of WBCs was assessed to determine the corresponding volume of functionalized magnetic NP that should be added to respect the ratio of 400 NP/WBC and 100 NP/WBC for anti-CD45 and anti-CD15 antibodies, respectively.

After this first pre-enrichment step, the sample was loaded in a 24-well plate for WBC magnetic labeling (30 min incubation at 37 °C under agitation). Next, the sample, containing magnetically labeled WBCs and A549 cells, was loaded into an eppendorf 1.5 mL tube and injected within the MagPure chip at 2 mL/h, which was priorly sterilized and Pluronic-coated.

After purification, the number of total cells and alive cells was again determined with Trypan blue and reported as a characteristic data of the magnetic-based purification.

Finally, the output of the whole workflow was collected for subsequent analysis, either for 2D cell culture and cell proliferation study, or for ALDH1 surface marker expression study via an IF assay. It should be noted that, with the integrated workflow, blood samples were processed in about 3-4h (~3h with ClearCell program P3, ~3h30 with program P1).

SI Figures and Tables

S4. Description of reported studies plotted in the article's Fig. 2

Table S3. Reported magnetic forces generated by a wide range of magnetic micro-source types.

Research group	Micro-source	Fabrication method	Force measurement method	Magnetic force	Ref
Mirowski et al.	Array of NiFe rectangles (1x3x0.03 μm^3)	N/A	Stokes drag force, Magnetic force microscopy (MFM)	35 pN (Stokes), 45 pN (MFM) @0.5 µm	[10]
Yassine et al.	NiFe disks (3 µm diameter, 30 nm thickness)	Electron beam physical vapor deposition	Finite element analysis (Comsol)	2.2 pN @2.2 µm	[11]
Hu et al.	NiFe disks (50 µm diameter, 100 nm thickness)	Sputtering	Finite element analysis (Maxwell 3D software)	0.1 nN @1.9 µm	[12]
Zhou et al.	NdFeB-PDMS-filled channel with rectangular structures (1000x500 μm^2)	Composite (NdFeB/PDMS = 2:1 w/w)	Finite element analysis (Comsol)	8 pN @5 µm	[13]
Zhou et al.	Fe-PDMS-filled channel with 60° isosceles triangle structures (1000 µm width)	Composite (Fe/PDMS = 2:1 w/w)	Finite element analysis (Comsol)	70 pN @20 µm	[14]
Jaiswal et al.	Array of diamond-shaped Ni structures (64 µm edge size, 200 nm height)	Thermal deposition	Finite element analysis (Comsol)	5 to 1 nN range @10-40 µm	[15]
Poudineh et al.	Array of circular-shaped Ni structures (272-470 µm diameter range, 1.5 µm thickness)	Sputtering	Finite element analysis (Comsol)	10 to 0.001 fN @5-25 µm	[16]
Toraille et al.	Array of NiFe rectangular cuboids (110x110 μm^2, 4 µm thickness)	Electro-deposition	Stokes drag force	27 pN @7 µm	[17]
Ponomareva et al.	Stripped NdFeB 5-µm thick film with zones of reversed magnetization	Sputtering and thermo-magnetic patterning	MFM	3.75-0.7 nN range @1.35-2.95 µm	[18]
Mekkaoui et al.	Array of chain-like Fe microstructures	Composite (5wt% Fe-PDMS)	Stokes drag force, MFM, Finite element analysis (Comsol)	1 nN @6 µm, 2-0.5 nN @7-10µm, 1.8-0.01 nN @6-20 µm	[19], [20]
Zeng et al.	Fe_3O_4 powder-filled channel (40-µm high) with a series of triangular structures (100 µm width, 50 µm height)	Ferrofluid (Fe3O4 powder mixed with pure water = 1:500 m/v)	Finite element analysis (Comsol)	1.3-0.01 nN range @0-5 µm	[21]

S5. Cell integrity study after processing through the MagPure chip

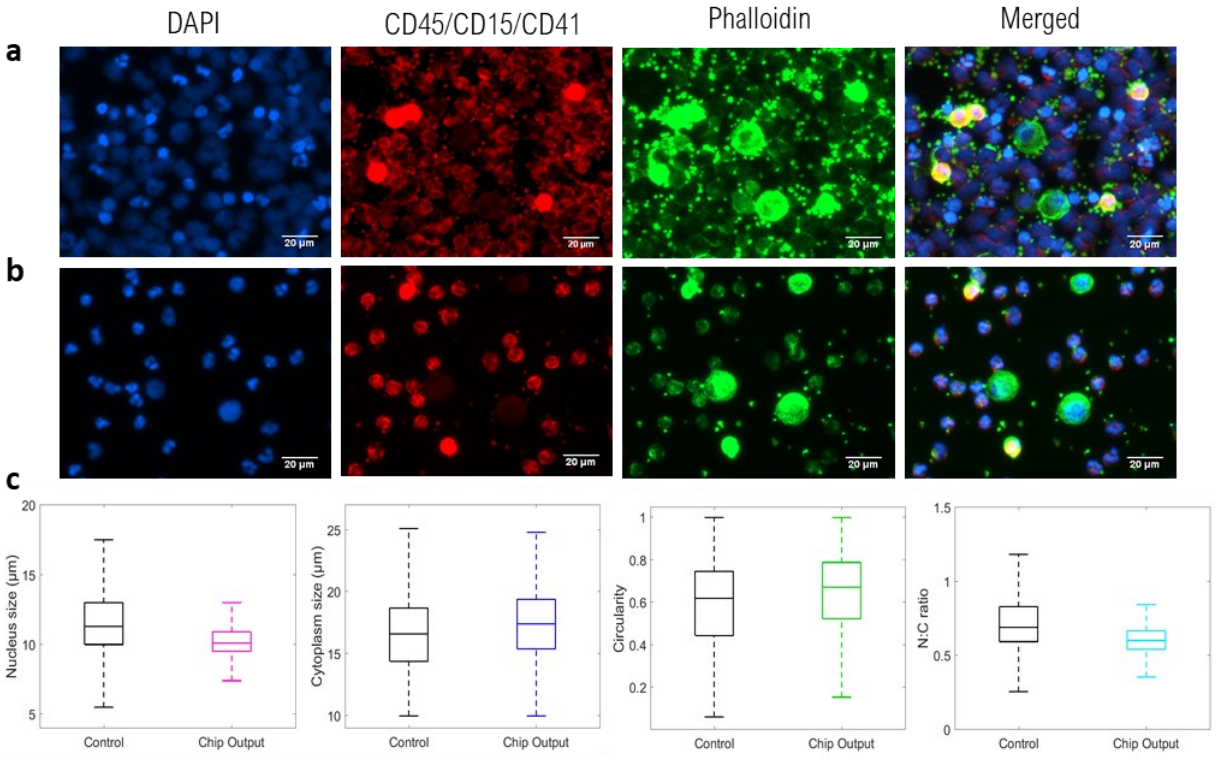

Fig. S1. Cell integrity investigation. Immunofluorescence staining for (a) control group (no purification step) and (b) recovered cells after magnetic separation. A549 cancer cells are determined according to DAPI+/CD45-CD15-CD41-/Phalloidin+. Benefit of the magnetic purification can be seen on the removal of excess background cells. On the control image (a), 2 A549 cells surrounded by ~100 background cells can be visualized (2% of cancer cells). On the collected sample post magnetic purification (b), 3 A549 cells and ~30 background can be observed (10% of cancer cells). (c) Morphological characteristics, including nucleus and cytoplasm sizes, circularity, and N:C ratio, obtained from immunofluorescence staining. Nucleus and cytoplasm sizes were determined by DAPI and Phalloidin fluorescent signals, respectively. 1,500 and 1,000 A549 cells were analyzed for control and chip output conditions, respectively.

S6. Long-term 3D cell culture after processing through the MagPure chip

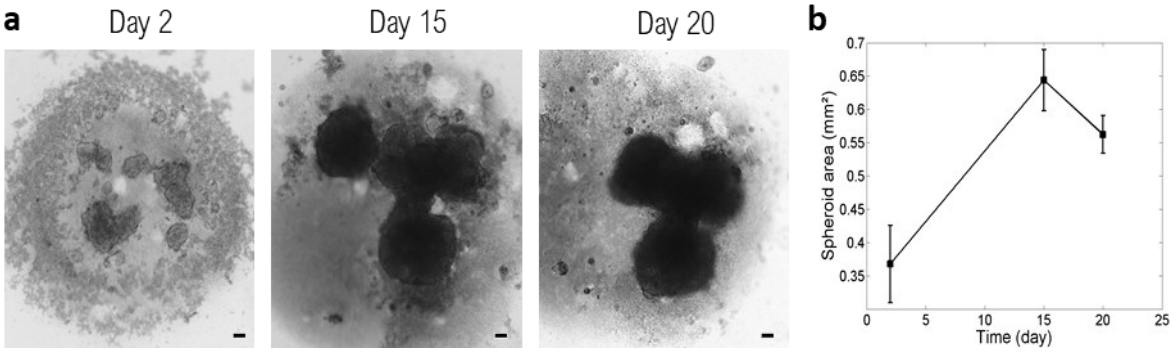

Fig. S2. Long-term spheroid culture. (a) Spheroid growth imaging and (b) spheroid area monitoring over 20 days. After two weeks of spheroid culture, spheroid area starts to decrease. Scale bars 100 µm.

S7. Long-term 2D cell culture after processing through the two-step workflow

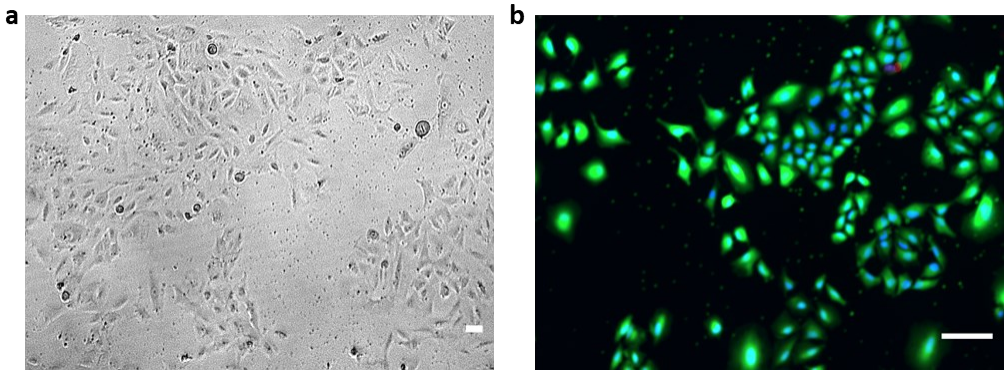

Fig. S3. Recovered cells after the whole workflow were cultured for 4 days before determining cell viability. **(A)** Phase contrast images showing cell re-adherence. **(B)** Fluorescence images obtained during Live/Dead assay. The viability rate, which was determined by analyzing 2,000 cells, reached 90%. Scale bars: 100 µm.

S8. Highlights on the challenges in size-based sorting methods

Challenges of the size-based sorting method were underlined after comparing the size of collected mCTCs with that of remaining WBCs (Fig. S4). Some of recovered A549 present a diameter comprised between 5 and 15 µm, like WBC diameter. This size overlap reveals the challenges in size-based sorting methods. Median diameter values are 13.9 µm and 10.3 µm, for A549 cells and WBCs, respectively. These values are consistent with ClearCell program P1 cut-off size (14 µm according to manufacturer's information) through which cells were first processed as the first size-based separation step. Thus, in theory, cells smaller than 14 µm are removed, but few cells escaped to this sorting parameter, including A549 cells. The additional immumomagnetophoretic-based purification step allowed for further WBC depletion, reducing their number by ~7.5 (from average 53,000 WBCs after P1 to 7,100 after the magnetic chip). This study highlights that, in addition to providing purified and viable cell samples, the magnetic chip enables the recovery of CTCs independent of their size or marker expression, which is highly requested given the reported heterogeneity of CTCs [22]–[24].

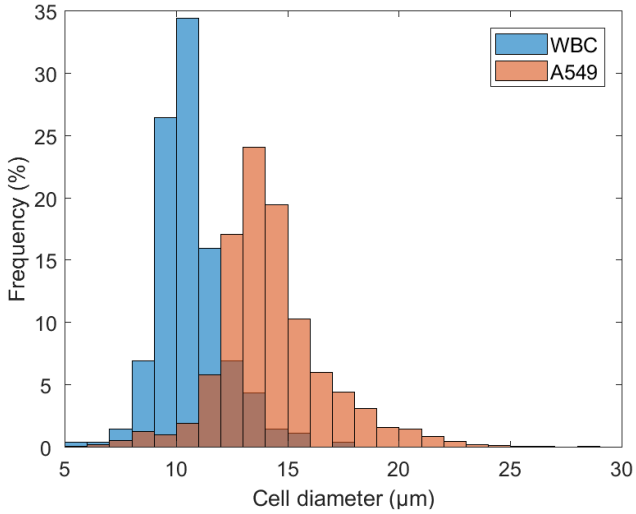

Fig. S4. Comparison of A549 cell diameter with WBC diameter. A549 diameter can be comprised between 5 and 15 µm, like WBC size, underlining the challenges in CTC isolation by size-based sorting methods. Analyzed cells were first processed with ClearCell program P1, followed by the magnetic purification step.

References

[1] E. Matijevic, *Medical Applications of Colloids*. 2008.

[2] E. Ozkumur *et al.*, “Inertial Focusing for Tumor Antigen–Dependent and –Independent Sorting of Rare Circulating Tumor Cells,” *Sci. Transl. Med.*, vol. 5, no. 179, pp. 1–20, 2013, doi: 10.1126/scitranslmed.3005616.Inertial.

[3] W. Zhao *et al.*, “Tumor antigen-independent and cell size variation-inclusive enrichment of viable circulating tumor cells,” *Lab Chip*, vol. 19, no. 10, pp. 1860–1876, 2019, doi: 10.1039/c9lc00210c.

[4] C. L. Chen *et al.*, “Separation and detection of rare cells in a microfluidic disk via negative selection,” *Lab Chip*, vol. 11, no. 3, pp. 474–483, 2011, doi: 10.1039/c0lc00332h.

[5] T. Y. Lee, K. A. Hyun, S. Il Kim, and H. Il Jung, “An integrated microfluidic chip for one-step isolation of circulating tumor cells,” *Sensors Actuators, B Chem.*, vol. 238, pp. 1144–1150, 2017, doi: 10.1016/j.snb.2016.05.163.

[6] P. M. Aldridge *et al.*, “Prismatic Deflection of Live Tumor Cells and Cell Clusters,” *ACS Nano*, vol. 12, no. 12, pp. 12692–12700, 2018, doi: 10.1021/acsnano.8b07616.

[7] Y. Takahashi *et al.*, “Integrated system for detection and molecular characterization of circulating tumor cells,” *PLoS One*, vol. 15, no. 8 August, pp. 1–13, 2020, doi: 10.1371/journal.pone.0237506.

[8] C. A. Aya-Bonilla *et al.*, “Detection and prognostic role of heterogeneous populations of melanoma circulating tumour cells,” *Br. J. Cancer*, vol. 122, no. 7, pp. 1059–1067, 2020, doi: 10.1038/s41416-020-0750-9.

[9] J. Garcia *et al.*, “Semi-automatic pd-l1 characterization and enumeration of circulating tumor cells from non-small cell lung cancer patients by immunofluorescence,” *J. Vis. Exp.*, vol. 2019, no. 150, 2019, doi: 10.3791/59873.

[10] E. Mirowski, J. Moreland, A. Zhang, S. E. Russek, and M. J. Donahue, “Manipulation and sorting of magnetic particles by a magnetic force microscope on a microfluidic magnetic trap platform,” *Appl. Phys. Lett.*, vol. 86, no. 24, pp. 1–3, 2005, doi: 10.1063/1.1947368.

[11] O. Yassine *et al.*, “Isolation of cells for selective treatment and analysis using a magnetic microfluidic chip,” *Biomicrofluidics*, vol. 8, no. 3, 2014, doi: 10.1063/1.4883855.

[12] X. Hu, S. R. Goudu, S. R. Torati, B. Lim, K. Kim, and C. Kim, “An on-chip micromagnet frictionometer based on magnetically driven colloids for nano-bio interfaces,” *Lab Chip*, vol. 16, no. 18, pp. 3485–3492, 2016, doi: 10.1039/c6lc00666c.

[13] R. Zhou *et al.*, “Fabrication and integration of microscale permanent magnets for particle separation in microfluidics,” *Microfluid. Nanofluidics*, vol. 20, no. 7, pp. 1–12, 2016, doi: 10.1007/s10404-016-1774-6.

[14] R. Zhou and C. Wang, “Microfluidic separation of magnetic particles with soft magnetic microstructures,” *Microfluid. Nanofluidics*, vol. 20, no. 3, pp. 1–11, 2016, doi: 10.1007/s10404-016-1714-5.

[15] D. Jaiswal, A. T. Rad, M. P. Nieh, K. P. Claffey, and K. Hoshino, “Micromagnetic Cancer Cell Immobilization and Release for Real-Time Single Cell Analysis,” *J. Magn. Magn. Mater.*, vol. 427, no. October 2016, pp. 7–13, 2017, doi: 10.1016/j.jmmm.2016.11.002.

[16] M. Poudineh, E. H. Sargent, and S. O. Kelley, “Amplified Micromagnetic Field Gradients Enable High-Resolution Profiling of Rare Cell Subpopulations,” *ACS Appl. Mater. Interfaces*, vol. 9, no. 31, pp. 25683–25690, 2017, doi: 10.1021/acsami.7b04677.

[17] L. Toraille *et al.*, “Optical Magnetometry of Single Biocompatible Micromagnets for Quantitative Magnetogenetic and Magnetomechanical Assays,” *Nano Lett.*, vol. 18, no. 12, pp. 7635–7641, 2018, doi: 10.1021/acs.nanolett.8b03222.

[18] S. Ponomareva *et al.*, “A quantitative study of magnetic interactions between a micro-magnet

array and individual magnetic micro-particles by scanning particle force microscopy," *J. Micromechanics Microengineering*, vol. 29, p. 015010, 2019, doi: 10.1088/1361-6439/aaefd5.

[19] S. Mekkaoui, "Développement de polymères composites auto-organisés pour la mise en œuvre de fonctions magnétiques en microsystèmes fluidiques," Université Claude Bernard Lyon 1, 2019.

[20] S. Mekkaoui, L. Descamps, M. C. Audry, A. L. Deman, and D. Le Roy, "Nanonewton Magnetophoretic Microtrap Array for Microsystems," *Langmuir*, vol. 36, no. 48, pp. 14546–14553, Dec. 2020, doi: 10.1021/acs.langmuir.0c02254.

[21] L. Zeng *et al.*, "Label-free separation of nanoscale particles by an ultrahigh gradient magnetic field in a microfluidic device," *Nanoscale*, vol. 13, p. 4029, 2021, doi: 10.1039/d0nr08383f.

[22] F. Fachin *et al.*, "Monolithic Chip for High-throughput Blood Cell Depletion to Sort Rare Circulating Tumor Cells," *Sci. Rep.*, vol. 7, no. 1, pp. 1–11, 2017, doi: 10.1038/s41598-017-11119-x.

[23] M. Poudineh *et al.*, "Tracking the dynamics of circulating tumour cell phenotypes using nanoparticle-mediated magnetic ranking," *Nat. Nanotechnol.*, vol. 12, no. 3, pp. 274–281, 2017, doi: 10.1038/nnano.2016.239.

[24] C. Renier *et al.*, "Label-free isolation of prostate circulating tumor cells using Vortex microfluidic technology," *npj Precis. Oncol.*, vol. 1, no. 1, p. 15, Dec. 2017, doi: 10.1038/s41698-017-0015-0.